TECHNICAL REPORT

Design and simulation of a 1 MeV, 100 mA parallel-fed capacitive coupled cascade industrial accelerator

M. Nazari,[a] **F. Ghasemi,**[b,1] **F. Abbasi**[a] **and O. HasanPour**[a]

[a]*Shahid Beheshti University, Radiation Application Department, Tehran, Iran*
[b]*Nuclear Science and Technology Research Institute, Tehran, Iran*

E-mail: fsghasemi@aeoi.org.ir

ABSTRACT: The construction of indigenous parallel-fed capacitive coupled cascade accelerators for industrial electron beam processing has been taken up at accelerator division of NSTRI at Iran atomic energy organization. This machine has been previously developed by Radiation Dynamics Inc. (RDI), IBA Industrial and High Voltage Engineering Europa B.V. (HVE) companies. Parallel-fed capacitive coupled cascade generators are reliable and high current sources of DC accelerators with many scientific, medical and industrial applications. We have selected this mechine because of some superiorities of that in comparison with many existing accelerators. These superiorities are as follows: compactness, simplicity, cheapness, having typically higher amount of beam current, wide range of beam energy and addressing many areas of applications. In this article, the main parts of a 1MeV, 100mA parallel-fed cascade industrial accelerator have been analyzed, designed and simulated. These parts are the electron gun, accelerating tube, voltage multiplier column (VMC) and some of the other components of the VMC. The electron gun is of a diode type with the Pierce configuration. Two electron guns with different cathode shapes have been designed and compared with each other. The intended cathode is a Dispenser type with a tungsten heater and porous tungsten matrix wich is impregnated with LaB6 and works in ambient vacuum of 10–7 Torr. The required current in our accelerator is about 100mA. For the next step, the accelerating tubes with different electrode geometries have been designed, simulated and compared with each other and the best geometry has been selected. For the VMC, we have tried to achieve a low ripple output DC voltage. The VMC has been analyzed and simulated with PSpice simulation software and optimum values of different parameters were achieved. We have tried to get the optimum values of the PSpice simulations by a mechanical design in CST Particle studio. At the end, the parameters of the mechanically designed VMC had a good accordance with the results from PSpice.

KEYWORDS: Accelerator modelling and simulations (multi-particle dynamics; single-particle dynamics); Accelerator Subsystems and Technologies; Beam dynamics; Instrumentation for particle accelerators and storage rings - low energy (linear accelerators, cyclotrons, electrostatic accelerators)

---

[1]Corresponding author.

Contents

1 Introduction

Parallel-fed capacitive coupled cascade accelerators are reliable sources of ion and electron beams for industrial radiation procesing. These generators are able to provide beam currents up to orders of magnitude higher than the most of DC accelerators. In these generators, the capacitors are made out of metallic plates. Therefore, in comparison with RF accelerators, the whole structure is simpler and less expensive. These accelerators cover energy range of 0.1 to 6 MeV and address many areas of applications. Radiation processing of wire and cable insulators, heat-shrinkable plastics, tire components and medical devices sterilization are some of these applications [1, 2]. The parallel-fed cascade (VMC) is a capacitive coupled multiplier, which uses diode rectification. This unit converts an input RF voltage into a low ripple output DC voltage [3].

The VMC comprises corona guards, DEE (RF) electrodes and diode stacks in a pressure vessel. Thanks to the low ripple output DC voltage characteristic, these accelerators are also widely being used for ion applications [4, 5]. We have designed a compact mechanical structure (accelerator), with suitable properties in a pressure vessel. The pressure vessel has been designed in order to withstand 14atm pressure of N2/CO2 (0.8/0.2) gas mixture. The electron guns of the different industrial electrostatic accelerators are similar.
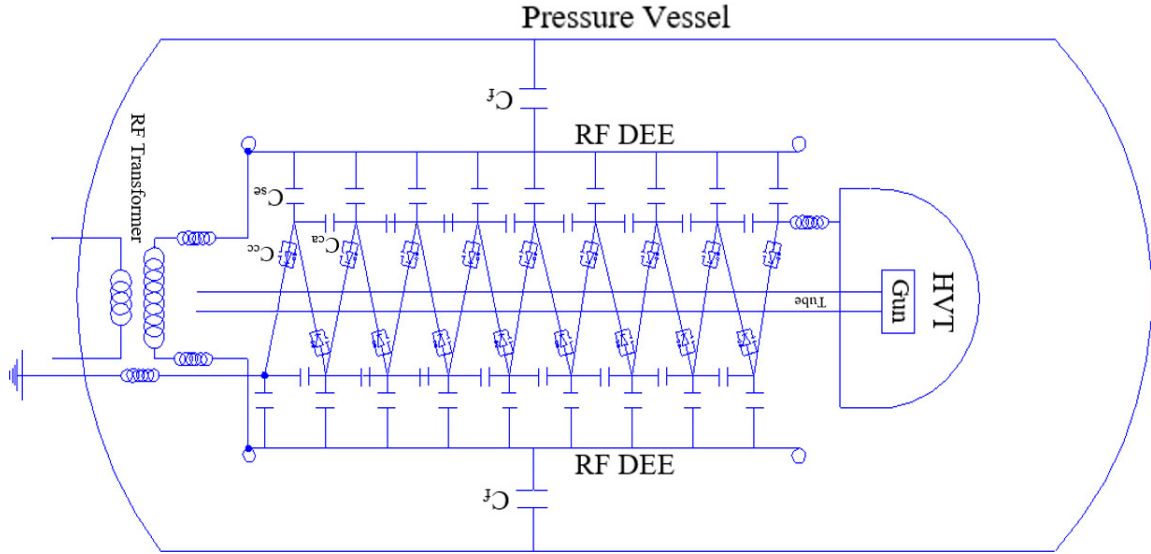
Figure 1. Schematic view of a parallel-fed capacitive coupled cascade accelerator and its components.

The concept of these guns is based on heating of a cathode or a filament as the cathode to reduce the work function and get a large amount of the electron beam. The information on several types of the thermionic electron guns is accessible in reference [6]. After creation of the particles, the array of electrodes which makes a uniform electric field, accelerates them along the tube [7].

2 Electron gun

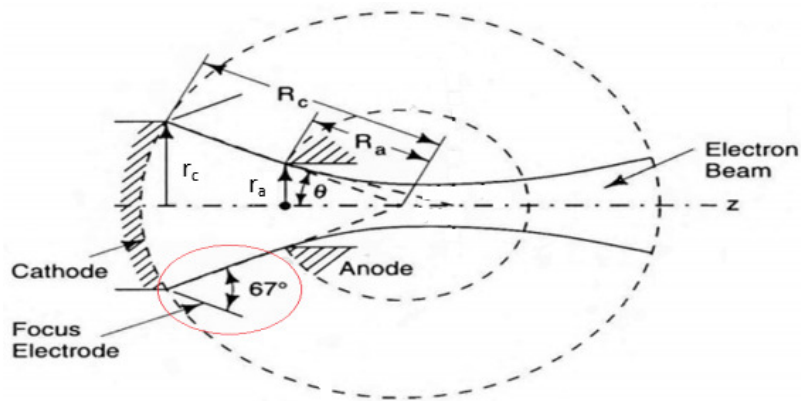### 2.1 Spherical Cathode Electron Gun

Figure 2. Schematic diagram showing anode and cathode parameters.

The first part which was designed is source of particles. In this part, we have designed a spherical cathode electron gun. Figure 2 shows a parametric schematic view of a spherical cathode electron gun [7]. In this type of electron guns, the emitted current (in space charge mode) is

calculated from equation (2.1) [8]:

$$I = 14.67 \times 10^{-6} \frac{(1 - \cos(\theta))}{(-\alpha)^2} V^{\frac{3}{2}} \qquad (2.1)$$

This equation is being known as Langmuir & Blodgett equation [8]. In this equation, V is the potential difference between anode and cathode and α is a coefficient, which is calculated from equation (2.2):

$$(-\alpha) = \gamma + 0.3\gamma^2 + 0.075\gamma^3 + 0.01432\gamma^4 + 0.00216\gamma^5 + 0.00035\gamma^6 \qquad (2.2)$$

γ is another numerical constant and is achievable by equation (2.3):

$$\gamma = \mathrm{Ln} \frac{1}{\left(1 - \frac{d}{R_c}\right)} \qquad (2.3)$$

R_C is the arc radius of the cathode and d is the distance between the anode and the cathode surface.

Another definable parameter in gun design is perveance, which is a numerical constant of electron guns in limited space charge mode. This parameter is just a function of the gun's geometry [9]. For the spherical cathode electron guns, the perveance is given by equation (2.4).

$$P = \frac{I}{V^{3/2}} = 14.67 \times 10^{-6} \frac{(1 - \cos(\theta))}{(-\alpha)^2} \qquad (2.4)$$
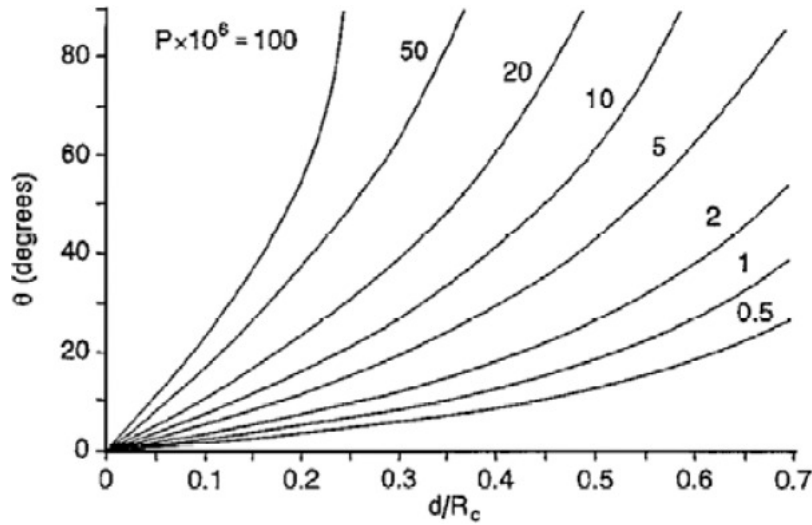

Figure 3. Perveance as a function of θ and anode-cathode gap [7].

The dimension of perveance is $A/V^{3/2}$ =microperv [7]. In RF linacs, for effective and efficient synchronization of input RF power with input electron beam from gun, and consequently reducing the beam loss, voltage of the electron gun is generally considered higher than that of the DC accelerators [10–12]. Unlike RF linacs, in a DC accelerator voltage gradient of the first section of the tube and the anode of the gun is low. Therefore, for DC accelerators, in most cases,

the gun voltage is not more than 10kV. On the other hand, the maximum value of the beam current of industrial parallel-fed electron accelerators is less than 300mA. Therefore, according to equation (2.4) perveance of the electron guns of these types of industrial accelerators is expected to be in 0.1–1 microperv range. Also in our designed gun, the values of d=15mm, Rc=25mm and θ=13° give us a perveance of about 0.25microperv. Figure 3 shows perveance as a function of θ and anode-cathode gap.

In almost all indirect heating cathodes, the heater is a filament of tungsten with a coating of alumina on it. This gun also has the same heater system.

For this filament, the temperature is predictable and adjustable by equation (2.5). According to this equation, the cathode temperature is just a function of the passed current through the filament wire [13]:

$$T = 735 + 1780I \tag{2.5}$$

Structural specifications of our designed spherical cathode gun have been shown and compared with that of the flat cathode gun in table 1. These values have been achieved from theoretical equations mentioned above.

Applying potential of 5kV between the anode-cathode gap in the simulation gives the equipotential lines of the gun in figure 4.
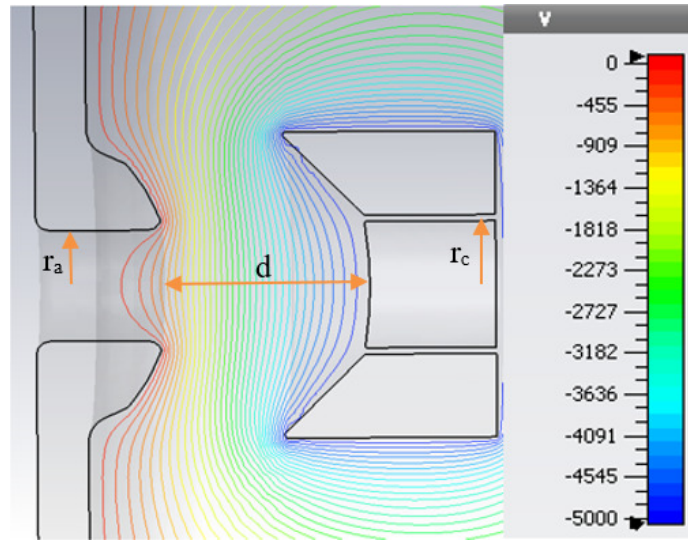

Figure 4. Equipotential lines in the anode-cathode gap.

The equipotential lines of the anode aperture have been bent toward the outside of the gun area. These bent lines create a defocusing lens in this area. Therefore, the beam current would be defocused by the anode aperture. Figure 5 shows the trajectory of the particles. The bending equipotential lines, at the surface of the cathode have focused the emitted beam current, into the anode aperture.

For changing the beam waist position and beam waist radius, the Pierce electrode angle should be suitably set [7].

According to figure 8, the beam waist radius and the beam waist position of the spherical cathode gun are about 2.3mm and 41mm respectively. Those profiles are recorded at behind of the
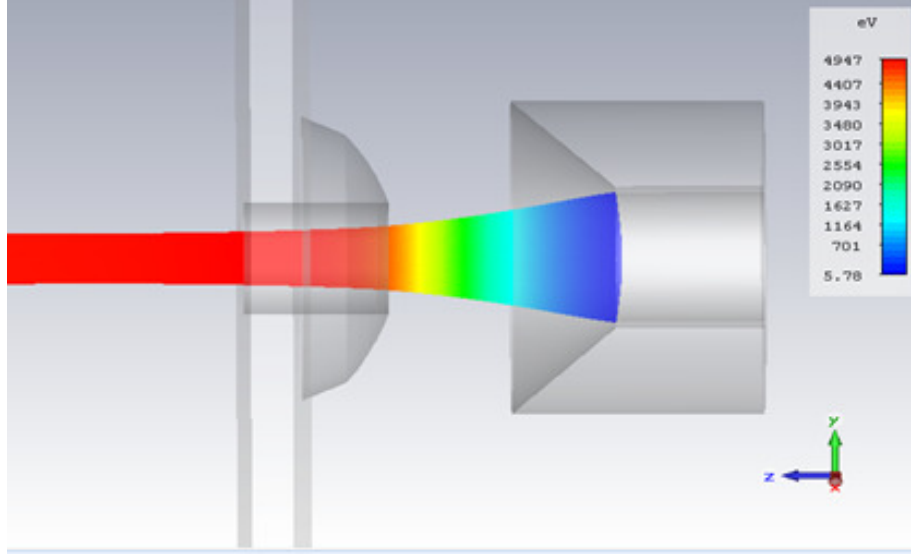
Figure 5. Particle trajectory in the designed spherical cathode electron gun.

anode aperture (at the beam waist position). The most of the particles have been focused toward the center of the gun axis. It means that our beam profile has a Gaussian distribution. This Gaussian distribution decreases the amount of the beam loss alongside the acceleration section.

As a conclusion we can state that the optimized characteristics of this designed electron gun that make it an appropriate selection for a DC electron accelerator are as follows: having Gaussian beam profile, appropriate beam waist position (41mm in comparison with d=15mm), appropriate beam waist radius (2–3mm for industrial applications) and a good perveance as an industrial gun.

2.2 Flat cathode electron gun

Another designed electron gun is a flat cathode type. This gun has the same current, voltage, perveance, anode-cathode gap distance and anode aperture as the spherical cathode gun. To make these parameters comparable, the cathode radius (r_c) of the flat cathode gun must be half of the spherical cathode gun radius. Therefore, we can compare these guns to each other. Based on our application, the comparable parameters are as follows: the beam waist position, beam waist radius, Gaussianity of the profile, stability of performance after a long time and cost [14, 15]. Figure 6 shows the schematic of the flat cathode Pierce electron gun.

In a flat cathode electron gun, the current density (in the space charge mode) is definable by equation (2.6):

$$J = 2.33 \times 10^{-6} \frac{V^{3/2}}{X^2} \tag{2.6}$$

In this equation, V is the anode-cathode potential difference and X is the anode-cathode gap distance. The perveance formula given by the equation (2.4) is also valid for the flat cathode electron guns. The specifications of the second designed electron gun have been shown in table 1:

The current density of the flat cathode has also been considered 1A/cm^2. The gun is designed Based on the theoretically calculated dimensions of the table 1. Figure 7 shows the beam trajectory of this gun.
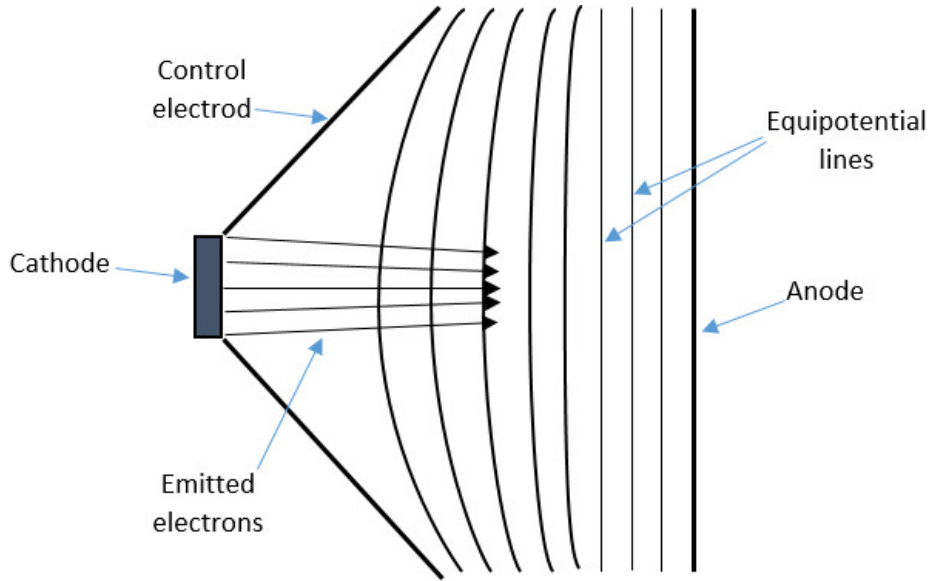
Figure 6. Schematic of the flat cathode Pierce electron gun.

Table 1. The specifications of the designed flat cathode and spherical cathode electron guns for space charge mode.

parameter	Value (spherical cathoide)	Value (flat cathode)
I	$0.246 \times 10^{-6} \mathrm{V}^{\frac{3}{2}}$	$0.246 \times 10^{-6} \mathrm{V}^{\frac{3}{2}}$
P	0.246microperv	0.246microperv
d	15mm	15mm
r_a	4.5mm	4.5mm
r_c	5.6mm	2.8mm
R_a	10mm	_
R_c	25mm	_
θ	13°	_
γ	0.916	_
α	1.235	_

All of the emitted particles from the surface of the cathode passed through the anode aperture and none of them hit the anode body. It also happened for the spherical cathode gun.

Figure 8 shows the overlapped beam profile of the flat cathode gun on that of the spherical cathode gun (both are at the waist position). The radius of the envelope of the particles is the beam waist radius. The beam waist radius and beam waist position of the flat cathode gun are 3.5mm and 21mm respectively. Both of the simulations (spherical cathode gun and flat cathode gun) have been done with the beam current of 87mA and the voltage of 5kV.
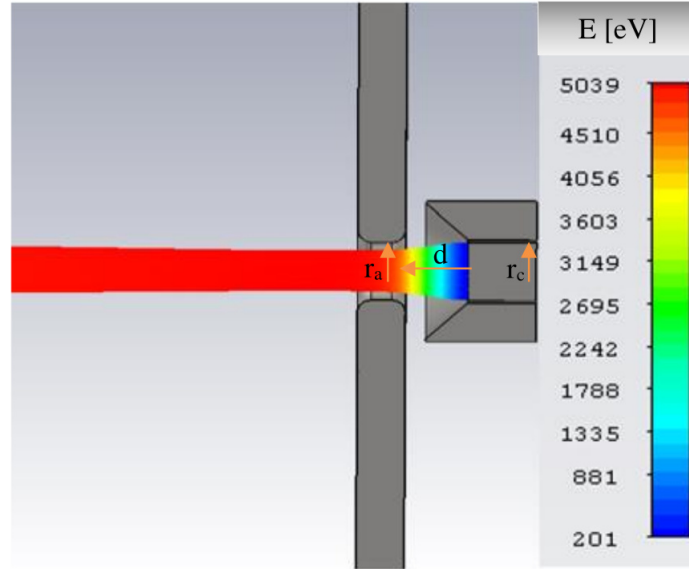
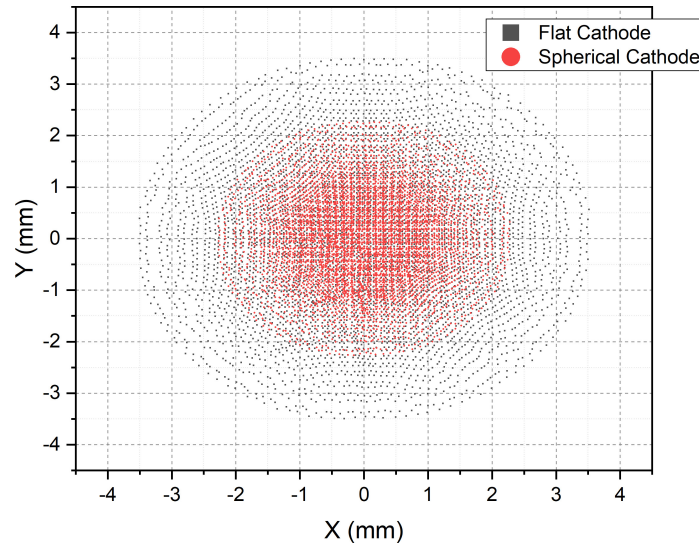**Figure 7**. Particle trajectory of the flat cathode electron gun.

Figure 8. Particle trajectory of the flat cathode electron gun.

Figure 8 obviously shows that the beam waist radius of the flat cathode gun is 1.2mm bigger than that of the spherical type. It should be mentioned that this amount is for the distance of 21mm (the beam waist position of the flat cathode gun) and at the distance of 41mm (the beam waist position of the spherical cathode gun), it will be more than 1.2mm. Figure 9 shows projection comparison of beam density in flat cathode and the spherical cathode gun.

As figure 9 shows, both of the profiles are Gaussian and the spherical cathode diagram is more focused than that of the flat cathode. Reasonably, the larger beam profile radius the more probability of collisions alongside the tube. Therefore, the spherical cathode gun is expected to have lower amount of the beam loss alongside the accelerating tube. Consequently, the beam dynamic
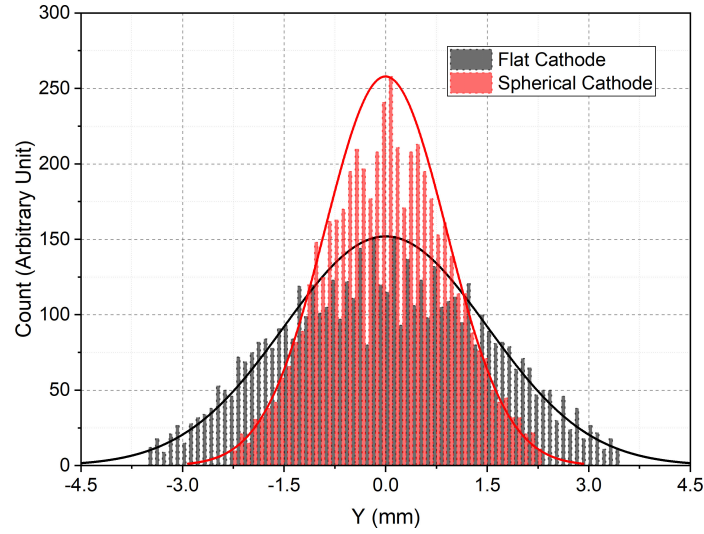
Figure 9. Overlapped projection of the beam density of the flat cathode gun on that of the spherical cathode gun.

characteristics of the spherical cathode guns make them more appropriate for research and more precise applications. Based on aforementioned comparisons, the spherical cathode guns have some superiorities over the flat cathode guns. In spite of these superiorities we have decided to select the flat cathode type. This is because, radiation processing is not a precise application and we should just use a 24/7 electron gun for a long period of time. Consequently we are not compelled to select the spherical cathode type. We also can use a simple replaceable direct heating tungsten filament [16].

3 Accelerating tube

After producing of the electron beam in the electron gun, it should be accelerated by an appropriate tube. In this section, we are going to discuss about three types of accelerating tubes. Based on our experience in the electrostatic accelerators, one of these geometries is used. Therefore, we have selected, studied and compared these three geometries to each other. Every electrostatic accelerating tube comprises two sections of focusing electrodes and accelerating electrodes. We have considered similar focusing electrodes for all of the three geometries. Based on our experience in the electrostatic accelerating tubes, the electrodes are made by aluminium, titanium or stainless steel and the insulators are made by glass or ceramic [17, 18]. In this project, we have decided to construct our tube by stainless steel and borosilicate glass.

3.1 Focusing electrodes

Focus electrodes and accelerating electrodes have different roles. Therefore, their mechanical structure is not similar. The focusing electrodes have adjustable potential and can adjust the beam dynamic characteristics of the tube, while the accelerating electrodes have constant potential and can only accelerate the particles [19, 20]. Figure 10 shows the first section of the tubes, including the insulators and the focusing electrodes.
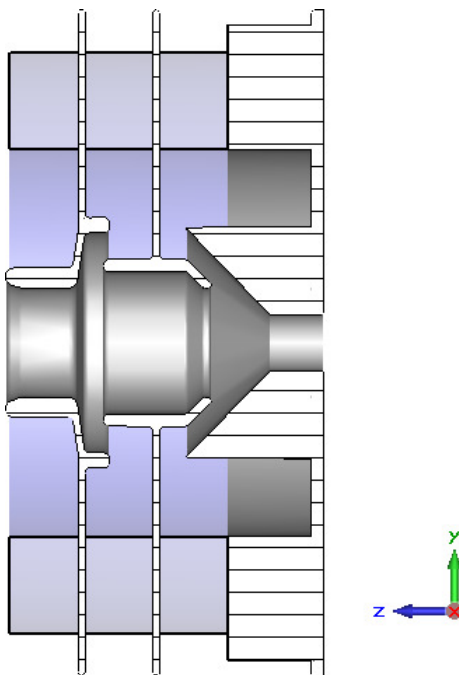
Figure 10. Mechanical structure of the first section of our designed accelerating tubes.
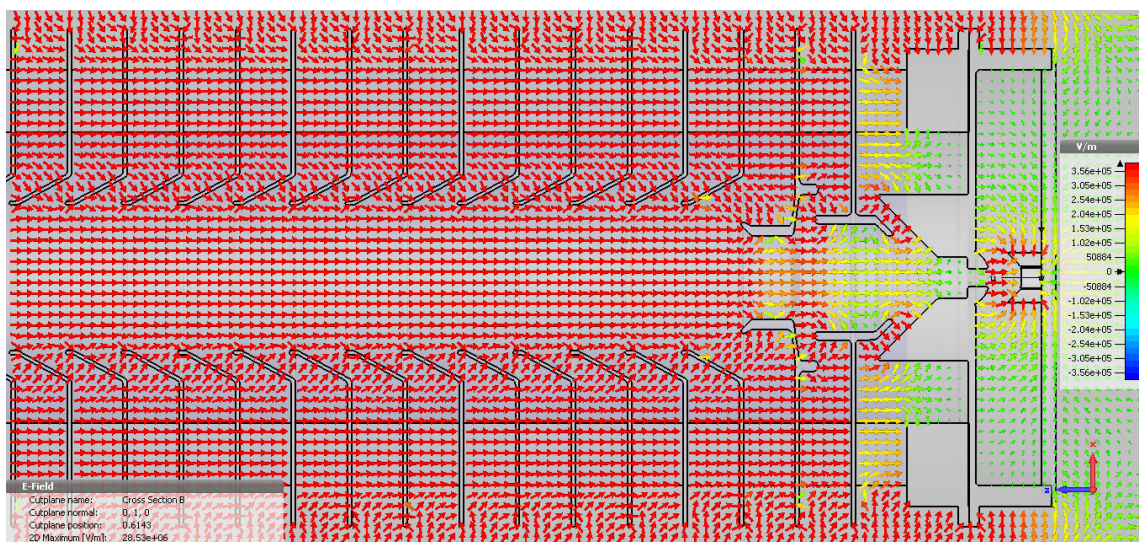

Figure 11. Distribution of electric fields at the first section of the tube.

The first part of the accelerating tube is designed for mounting the tube, on the electron gun. This part has the inlet radius of 10mm, the outlet slope of 45° and the length of 46mm (from the inlet to the outlet). Figure 11 shows the electric field lines in the first section of the tube.

We can see that the electron gun case has been isolated from the electric fields of the tube. Changing the potential of the first and the second focusing electrode acts as a lens and adjusts the output beam shape from the electron gun. For effective coverage of the insulator (mounted between

these two electrodes) from particle collisions, the second focusing electrode has an overlap (2mm) on the first focusing electrode. In addition, we must design our electrodes so that the array of the electrodes covers and protect the insulators [21, 22].

3.2 Accelerating electrodes

There are many different effective parameters in designing of an electrostatic accelerating tube which we can discus about them. Some of these parameters are beam loss on tube electrodes, halo formation, beam envelope changes with the beam current and the focusing electrodes potential, maximum sustainable electric field gradient, uniformity of longitudinal electric field, lifetime of the tube, tube length and cost. For designing a 24/7 industrial accelerating tube, the most important factors are beam loss on tube electrodes, maximum sustainable electric field gradient, uniformity of longitudinal electric field, lifetime of the tube, tube length and cost. Reference [23] has explained about current losses, secondary particle flows, beam halo formation and operation stability, in an electrostatic accelerating tube in details.
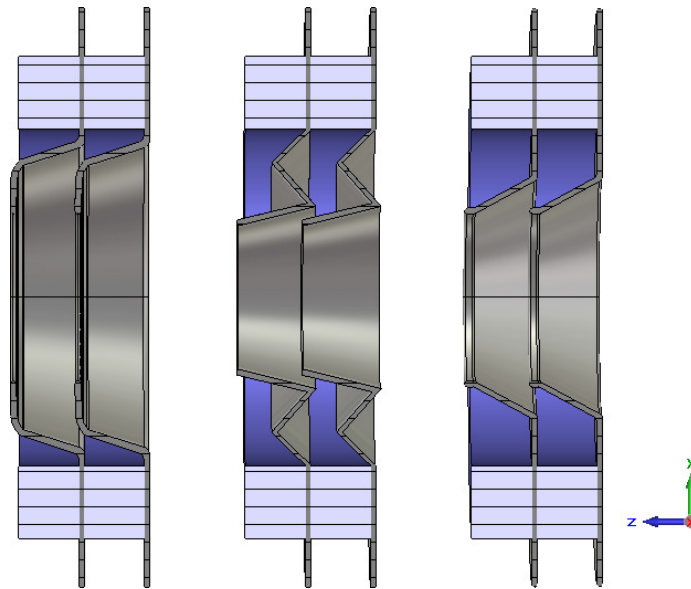

Figure 12. Different designed accelerating electrodes.

Some examples of beam loss mechanisms are beam halo formation, particles source fluctuations or turn on/off transients, residual gas stripping and dark current from the particles source. A well-known source of beam loss in accelerators is beam halo or long tails on the beam distribution. When the halo/tails intercept the tube apertures, the beam is lost. A certain level of halo/tail formation is inevitable. The halo/tails can be present from the very beginning (at the exit of the particles source) or they can be created by space charge, mismatched beams and in addition structure resonances, parametric resonances and Magnet imperfections in RF accelerators. Residual gas stripping can also cause significant beam loss during the commissioning phase, but we can mitigate it by Improving vacuum. Besides, current losses occur whenever the energy gain per gap is high in comparison to the particle energy. Due to sharper increase of electric field at the input of the RF accelerating tubes, the beam loss in RF accelerators is much more than DC accelerators. Capture coefficient for

standing wave and traveling wave accelerating tubes is about %30 and %80 respectively. The rest of the particles return toward the cathode surface and cause a back-bombardment. Unlike the RF accelerators, in DC accelerators the emitted particles after leaving the anode aperture will be faced with a very smooth electric field slope [12, 24]. Consequently based on our simulations the beam loss will not be more than 5 percent. In this article, we discuss about three types of accelerating tubes with different geometries. The designed accelerating electrodes, including the first (left side), the second (center) and the third geometry (right side) have been shown in figure 12.

In all geometries, the outlet radius is 35mm (left side aperture). The inlet radius (right side aperture) is different for everyone. There is a compromise between the maximum electric field gradient of the tube and the gap distance between two consecutive electrodes. Based on our simulations and case studies, for the gap distance of 25mm, longitudinal electric field distribution of the tube is uniform and smooth enough (figure 14). Increase of the distance decreases the electric field uniformity (figure 15) and the beam loss in the tube. On the other hand, decrease of this distance, increases the electric field gradient and probability of spark creation. This also creates some physical and mechanical problems and limitations on connection of the voltage divider connectors on tube electrodes.
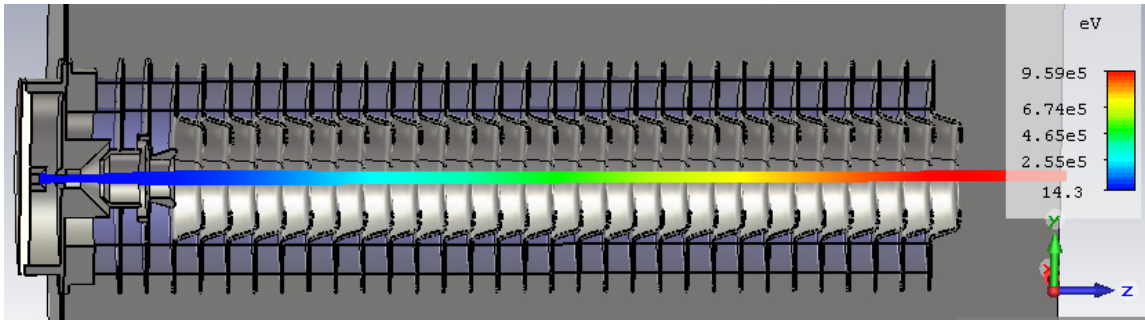

Figure 13. Trajectory of particles along the first geometry.

We have set 29 accelerating electrodes, 2 focusing electrodes and a single part (mounting electrode on the head of the tube) for achieving the energy of 1MeV. Thickness of the electrodes and the insulators is 2mm and 25mm respectively. Therefore, the tube length is 1 meter. We have applied equal potential steps of 35kV. The focusing electrodes have varying DC potentials. The second accelerating electrode has the potential of -945kV. To achieve more uniform electric field distribution, at the first section of the tube, the first accelerating electrode does not follow the step of -35kV. Therefore, instead of -980kV the potential of -965kV has been applied to this electrode. Figure 13 shows trajectory of the particles in the first geometry. This geometry has been used in 3MeV Van De Graff accelerator of Iran's Atomic Energy Organization.

Instability of the terminal voltage, frequency of the over voltages and created sparks in the VMC, create some fluctuations on beam current and current passed through the tubes' voltage divider. These fluctuations increase the beam loss in the tube. Lost particles hit the electrodes, charge the tube insulators and provoke partial discharges in the tube. Also, the frequency of these partial discharges increase the probability of the tube breakdown [23]. In addition, we have to design our electrodes in a way that completely shield the insulators from primary and secondary particle collisions. Consequently, we have to create some sharp curves and edges. These sharp

points increase the probability of producing sparks between the electrodes. Therefore, we have to implement some spark gaps between consecutive electrodes to compensate this problem, release the charge of the electrodes and insulators and remove the probability of the tube breakdown. Based on our simulations, the electric field distribution of the first and the third geometries are smoother than that of the second geometry. Therefore, we expect a more stable and uniform longitudinal electric field distribution, inside these geometries. Figure 14 also shows the longitudinal electric field distribution of the first geometry.
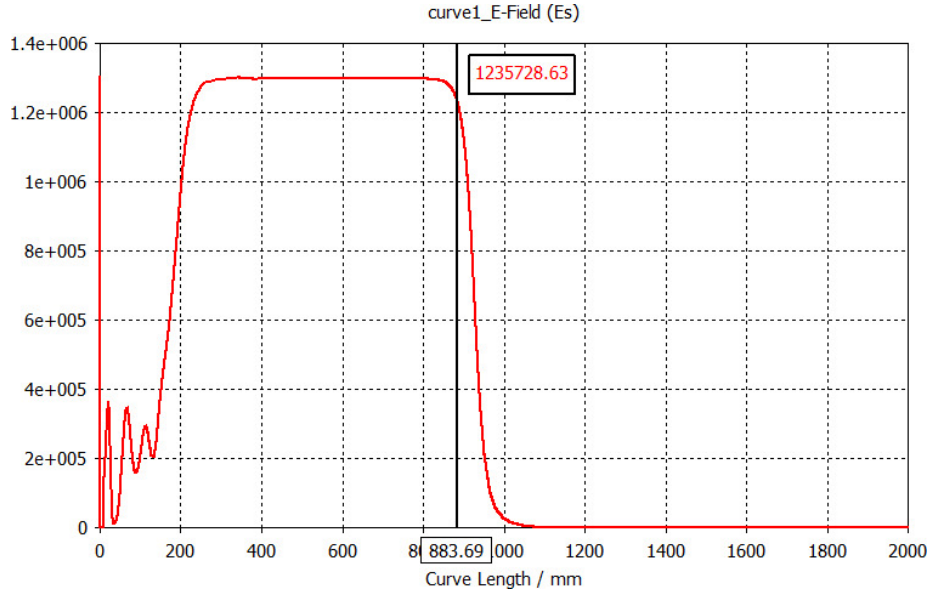

Figure 14. Longitudinal electric field distribution of the first geometry.

This diagram shows the uniformity of the electric field distribution, along the first tube. This uniformity causes the particles to experience a constant acceleration voltage. We can calculate earned energy of the electrons along the tube length. Magnitude of the electric field is almost 1.3MV/m and the length of the flat area (of the accelerating electrodes) is almost 700mm. Therefore, the earned energy of the particles in this part is:

$$\nabla d = d_2 - d_1 = 900 - 200 = 700 \, \text{mm}, \qquad E = 1.3 \times 10^6 \rightarrow U = 910 \, \text{keV}$$

The rest of this energy (90keV) comes from the first and the end sections (fluctuations) of the tube. The fluctuations in the initial part of the tube (0–200mm) are because of the electric potentials of the cathode, anode, the first focusing electrode and the second focusing electrode respectively. Likewise, the fluctuation of the end section (750–1000mm) is because of the smooth decreasing rate of the electric field at the end electrode and the beamline length.

As mentioned, one of the important parameters for an electrostatic tube is the gap between the electrodes. Figure 15 shows the longitudinal electric field distribution of the first tube, for the gap of 50mm instead of 25mm.

As expected, this diagram shows significant fluctuations of the electric field along the tube axis. These fluctuations defocus the envelope of the particles from the axis of the tube. Consequently,
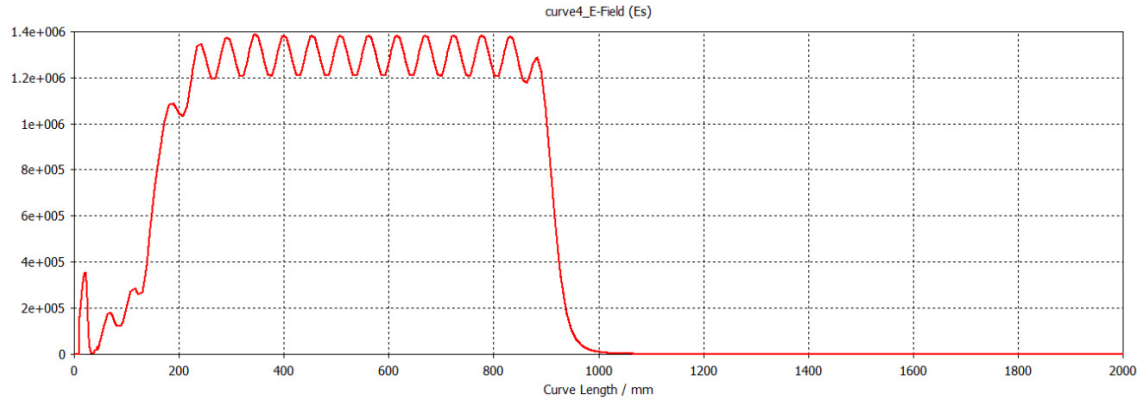
Figure 15. Fluctuations of the longitudinal electric field along the tube length for electrode gap distances of 5cm.
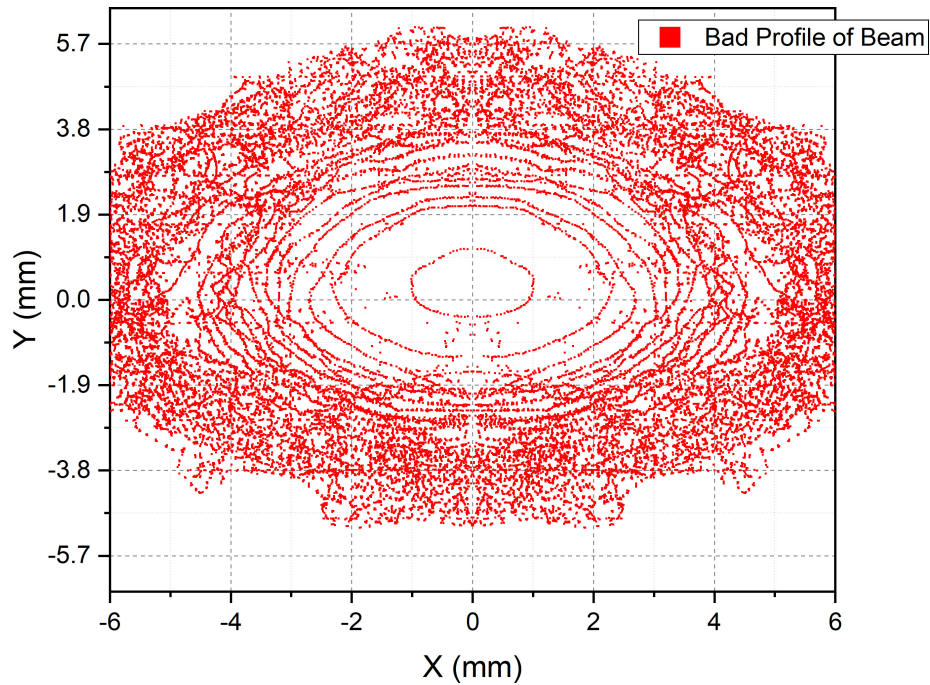

Figure 16. Output profile of the particles for electrode gap of 5cm.

the defocused profile causes a non-uniformity in radiation processing. The electric field gradient in both simulations of the figure 14 and 15 is adjusted the same. In this simulation, the tube had 15 Nos. of accelerating electrodes (with a potential step of 70kV), the same two focusing electrodes, tube length (1 meter) and energy. If we do not apply any beamline (drift tube) at the end section of the tube, there we be an aggregation of astray electric fields and consequently there will be a fluctuation instead of this smooth decreasing rate of the electric field. Figure 16 shows the output beam profile of the tube, for the gap of 50mm.

This profile shows that the output particles have lost their Gaussian profile and consequently have been dispersed into the marginal areas. It means that this structure will extremely increase the
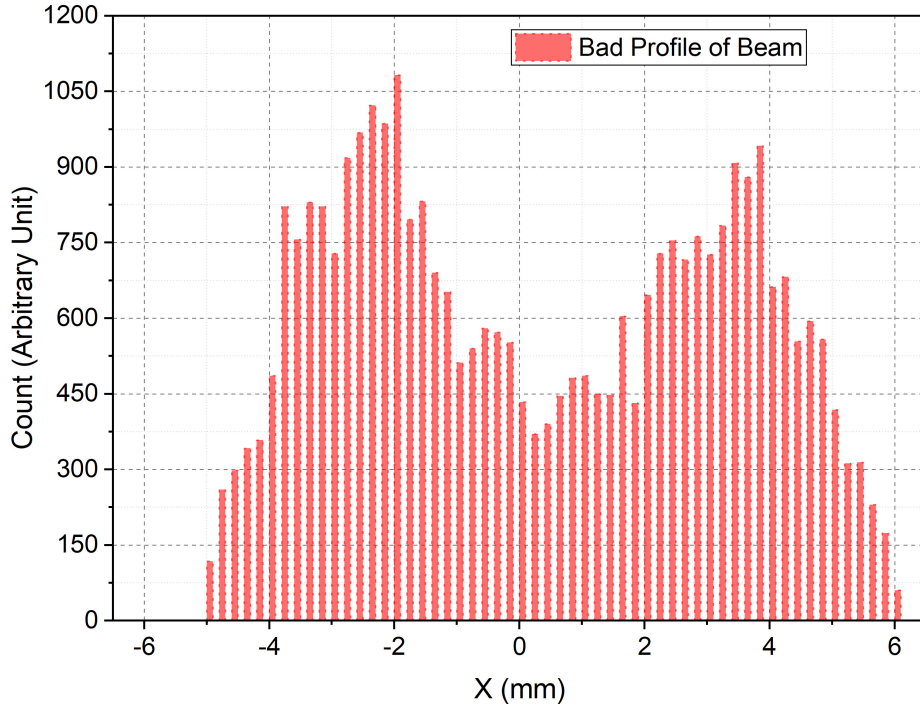
Figure 17. Abnormal particle distribution due to extra electrode gap distance.

particle loss of the tube and therefore the lifetime of this tube would be less than usual. Figure 17 shows the projection of the beam density of this profile at the output of the tube.

Studies and simulations of the longitudinal electric field distribution of the other two tubes also represents almost the same result which means that uniformity of the longitudinal electric field in all geometries is good enough. In addition, it depends on the gap distances of the electrodes more than the shape of them. The other important parameter is the amount of the beam envelope changes at the end of the different tubes with change of the focusing electrodes potential. In these simulations, we swept the potentials of the focusing electrodes in CST and Simion and compared the output result of different tubes. Figure 18 shows some of these changes, simulated by CST and Simion and table 2 shows the result of these simulations.

CST is a powerful 3D software with ability of combining time variant and static electric and magnetic fields in the same simulation. Unlike CST, Simion is a 2D software, which can only perform electrostatic or magnetostatic simulations apart from each other. In table 2 radius of the beam envelope (per mm) for different amounts of the focus electrodes potentials is shown.

Based on the results of the table 2 Simion simulations verify CST results, but there is a little difference between them. This difference is mostly because of the different amount of applied space charge effect in two softwares. With respect to our application, the output scanning window should provide the electron beam width of up to 1m. In addition, for an uniform and effective electron beam processing the output beam at the end of the tube should not be needle shaped. Therefore, we prefer the first and the second geometry to the third type.

Besides, in the third tube, protection of the insulators from the particle collisions is not as effective as the first and the second tube. Consequently, in high current applications, it would be
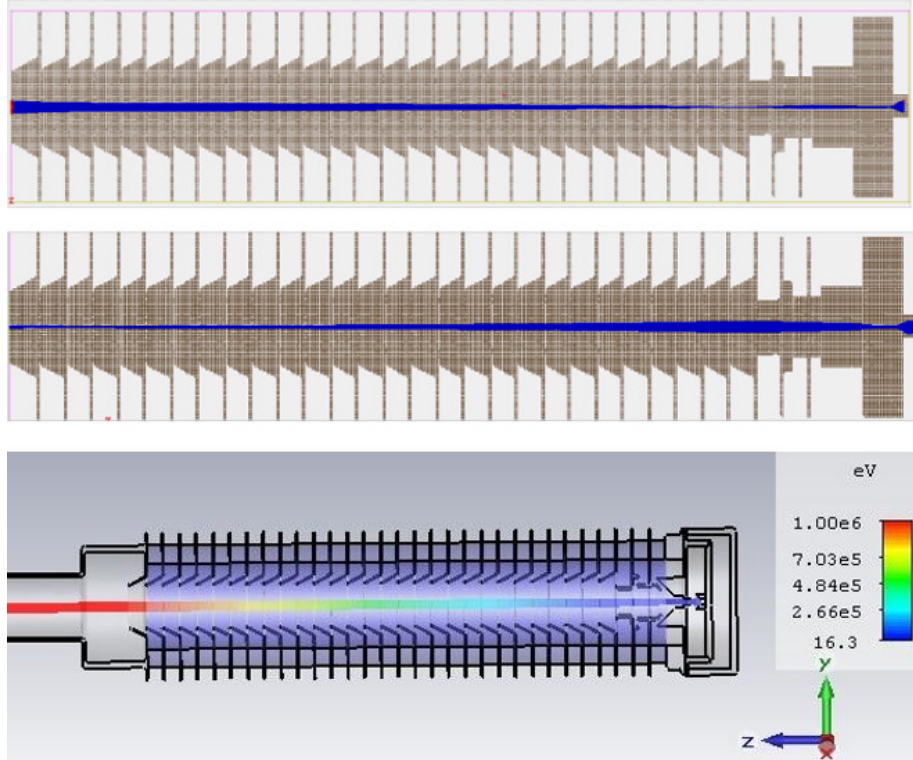
Figure 18. Beam envelope changes with changes of the focus electrodes potential, simulated by CST and Simion.

Table 2. Beam envelope changes at the end of the different tubes with change of the focusing electrodes potentials, simulated by CST and Simion.

First focus electrode potential (kV)	-995	-990	-985	-980	-975
second focus electrode potential (kV)	-985	-980	-975	-970	-965
first tube (radius of envelope (mm)) by CST	4	6	7	9	13
second tube (radius of envelope (mm)) by CST	2	4	6	9	11
third tube (radius of envelope (mm)) by CST	2	3	3.5	5	6
first tube (radius of envelope (mm)) by Simion	3	4.5	6	8	10
second tube (radius of envelope(mm)) by Simion	2	3	4.5	6	8
third tube (radius of envelope (mm)) by Simion	1	1.5	2	3.5	4.5

more vulnerable than the other geometries. Therefore, this structure is more appropriate for low energy and low current accelerators. This geometry has been used in several Cascade accelerators with energies of 150 to 200 keV in Iran. In addition, table 2 represents almost equal results for the first and the second tubes. In the first tube and mostly in the second tube the insulators have a good protection against the particle collisions. Therefore, both of these geometries are appropriate for our application. Consequently, we selected the first geometry for our tube because of uniformity of elec-

tric field distribution, good protection of the insulators, simplest electrode structure in comparison with the second tube, and our previous experiences in working with one of these tubes in Iran.

Another important factor in constructing an electrostatic tube is the alignment of tube components. The deflected electrons hit the tube body and cause damages on it. Therefore, a little misalignment can cause a certain damage in the tube structure. For studying the amount of transvers deviation of the beam trajectory, we applied a dislocation of 2mm on every electrode of the tube in transvers direction. Table 3 shows the result of these studies.

Table 3. The effect of misalignment of different electrodes on the beam trajectory.

Misaligned Electrode	Beam deflection from the tube axis (mm)
First focusing electrode	4.4
Second focusing electrode	4.4
First accelerating electrode	0.5
Second accelerating electrode	0.3
Third accelerating electrode	0.2
The next accelerating electrodes	<0.1

Table 3 shows that alignment of the first and the second focusing electrodes is more important than the other electrodes. In fact, increase of the energy of the particles, increases momentum and rigidity of the particles along the tube length and consequently decreases the effect of these misalignments on particles. Therefore, in the construction process, alignment of the first section of the tube is more important than the accelerating section.

4 Voltage multiplier column

This part is in fact the same improved Greinacher circuit, But with parallel feeding of the capacitors [25, 26]. The output DC voltage, voltage drop and the voltage ripple of this VMC can be calculated by the following equations [27].

$$U = \frac{NU_0}{k} - U_{\text{droop}} \pm U_{\text{ripple}} \tag{4.1}$$

$$U_{\text{droop}} = \frac{I(N-1)}{fC_{\text{Se}}k} \tag{4.2}$$

$$U_{\text{ripple}} = \frac{I}{2fC_{\text{Se}}} \tag{4.3}$$

$$k = 1 + 4\frac{C_{\text{Ca}}}{C_{\text{Se}}} \tag{4.4}$$

In these equations, k is known as coupling coefficient, C_{ca} is the shunt capacitance and C_{se} is the coupling capacitance. Figure 19 shows a part of the VMC circuit and its components, simulated in PSpice software.

C_{se} = capacitance between corona guard and RF electrode

C_f = capacitance between RF electrodes and the pressure vessel

C_{CC} = capacitance between two parallel corona guards

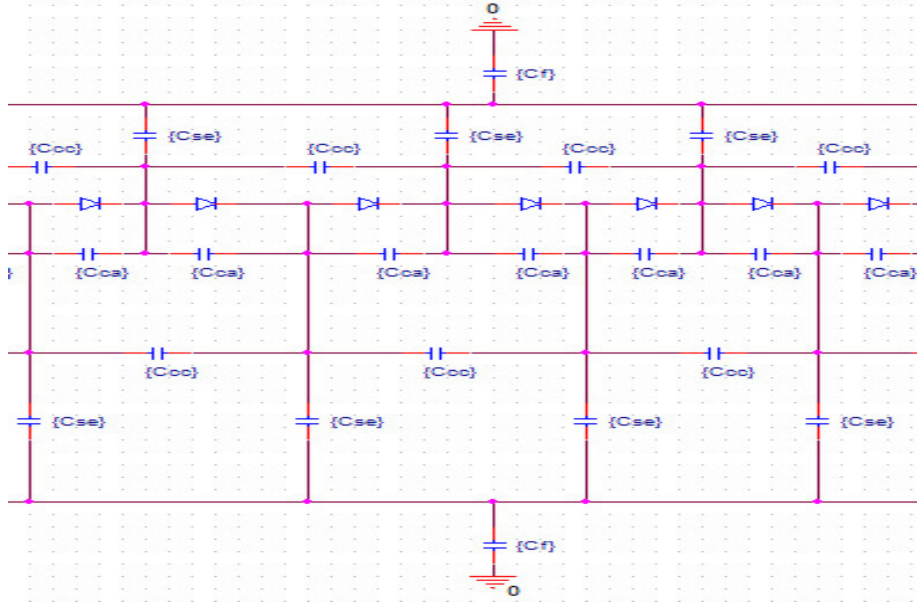C_{ca} = capacitance parallel with every diode stack

Figure 19. A part of the simulated parallel-fed circuit, simulated by Pspice.

With respect to the equations of (4.2) and (4.3), the terms of U_{droop} and U_{ripple} are adversely related to the frequency of the input RF voltage. Therefore, in this circuit the frequency range is an important factor. Figure 20 shows the effect of frequency change (simulated from 100kHz to 200kHz) on the voltage ripple and the output DC voltage [28].
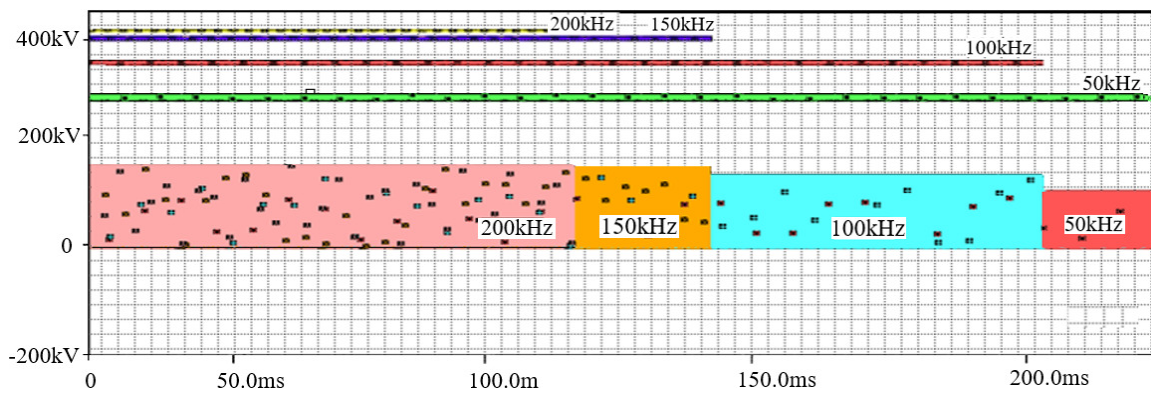

Figure 20. Sweep of the frequency from 100 kHz to 200 kHz.

According to this simulation, upper frequencies cause a lower ripple and a higher DC voltage. In the equal condition, Green curve (50kHz) shows about a DC voltage of 300kV while blue curve

(150kHz) shows about 400kV. Besides, the ripple of the green curve is more than that of the blue curve. Wide curves (with zero baseline), show the applied potential difference on every diode stack in different frequencies [29].

In addition to these parameters, the power loss of the RF transformer also depends on the frequency of the RF voltage. With respect to all the mentioned points, in Practice the suitable frequency range of the input RF voltage is selected between 100kHz-150kHz [30]. In these frequencies, the reverse recovery time of the diodes should be lower than 100ns.

5 Design and simulation of the 1 MeV, 100 mA parallel-coupled capacitive cascade accelerator
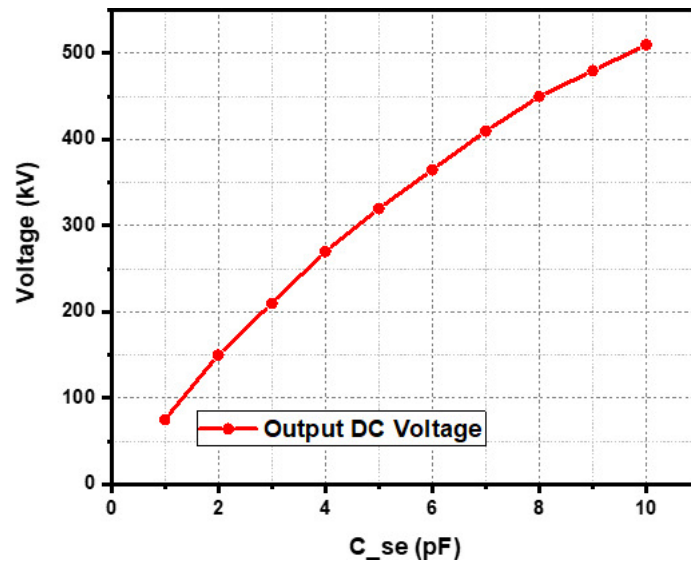
5.1 Optimization of capacitors

Figure 21. Effect of Cse on the output DC voltage of the parallel-fed circuit.

In the following section, we study the effects of the changes in values of the different capacitances of the circuit on the output DC voltage and voltage ripple of the VMC by PSpice simulations. Figure 21 shows the output DC voltage as a function of Cse.

Increase of C_{se} from 1pf to 10pf, increases the DC voltage from 75kV up to 500kV. This curve represents a linear relation between capacitance of C_{se} and the output DC voltage.

Increase of the capacitance of C_{se}, causes a sharp increase in the DC voltage of the circuit. Therefore, for achieving higher output DC voltages, we should increase the capacitance of C_{se} as much as possible. In the other hand, large values of this capacitance in practice has three disadvantages of: 1) increase of the equivalent capacitance of the VMC and therefore increase of the stored energy of the column 2) increase of the passed forward current through the diodes 3) changing of the output DC voltage to a pulsed DC voltage.

The more stored energy creates the more sparks and instabilities in the VMC. Next discussion is about the effect of the capacitance of C_{se} on the output voltage ripple of HVT. Figure 22 shows
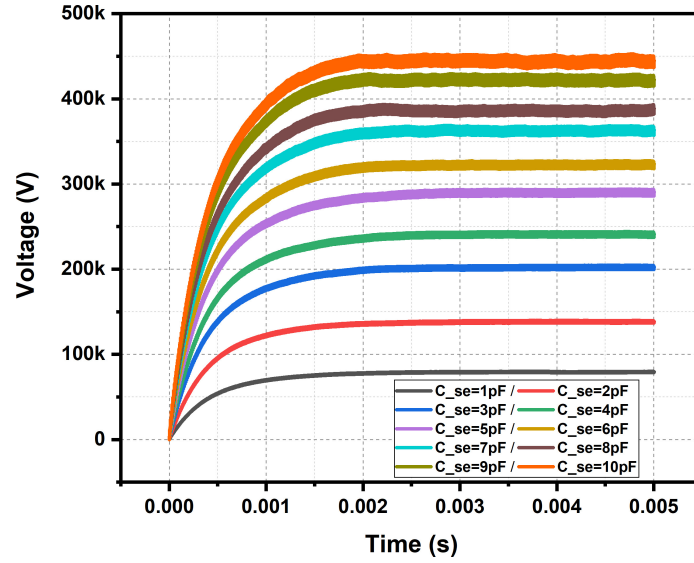
Figure 22. Voltage ripple of the circuit as a function of Cse value.

changes of the output DC voltage from the same stage of the circuit, for different values of C_{se} from 1pf to 10pf.

According to the equation (4.3) in no-loud condition (I=0) for different amounts of C_{se} the output voltage ripple is zero. We can hold the output current (I) to a constant value by regulating the loud of the circuit. Under this condition, increase of C_{se} leads to increase of the output DC voltage and decrease of the voltage ripple. In another condition (figure 22), we apply a constant loud and increase the capacitance of C_{se}. This condition leads to increase of the output DC voltage and the current of the circuit and consequently increase of the voltage ripple. Therefore, we see higher values of voltage ripple on higher levels of the output DC voltage in figure 22. The second effective element for the VMC is the capacitance of C_{ca}. Figure 23 shows the output DC voltage as a function of C_{ca} (from 1pf to 10pf).

According to the theoretical and simulation results, the capacitance of C_{ca} is inversely proportional to the output DC voltage. Therefore, for getting higher output DC voltages we should decrease the capacitance of C_{ca} as much as possible. In fact, because of the junction capacitance of the diodes, created cross capacitance between the corona guards and the capacitance between spark gaps of the corona guards, this parameter will inevitably increase. In addition, this capacitance acts as the impedance of the circuit and is necessary for getting higher values of current. Besides, according to the equation (4.3) and our simulations, the output voltage ripple is independent of capacitance of C_{ca}. Figure 24 shows the output DC voltage of the same stage of the circuit for different values of C_{ca} (from 1pf to 10pf).

With respect to this simulation, the capacitance of C_{ca} affects sharply on the output DC voltage and higher values of C_{ca} leads to lower values of the output DC voltage. Therefore, for getting higher values of output DC voltage, C_{ca} should be kept down.

The third issue is about the capacitance of C_{CC}. Based on theoretical equations and our simulations, the output DC voltage and voltage ripple of the VMC are independent of C_{CC} value. C_f is the last capacitance of the VMC that we study. Figure 25 shows the output DC voltage of the circuit for different values of C_f (from 1pf to 1000pf).
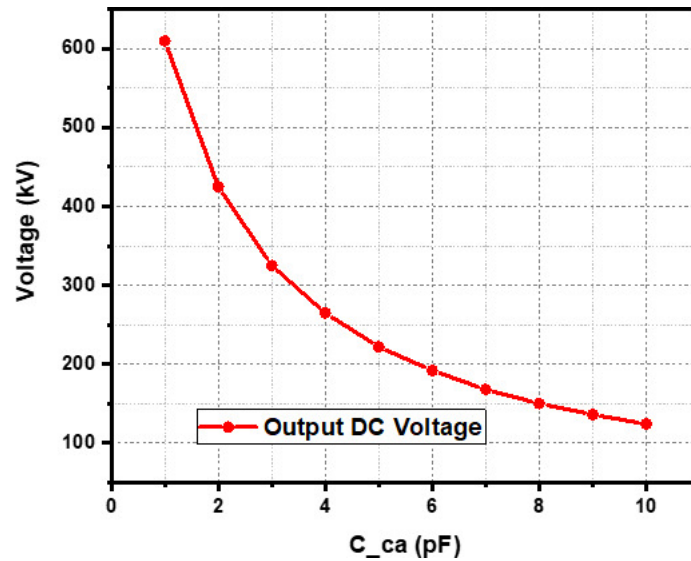
Figure 23. Effect of C_{ca} on the output DC voltage.
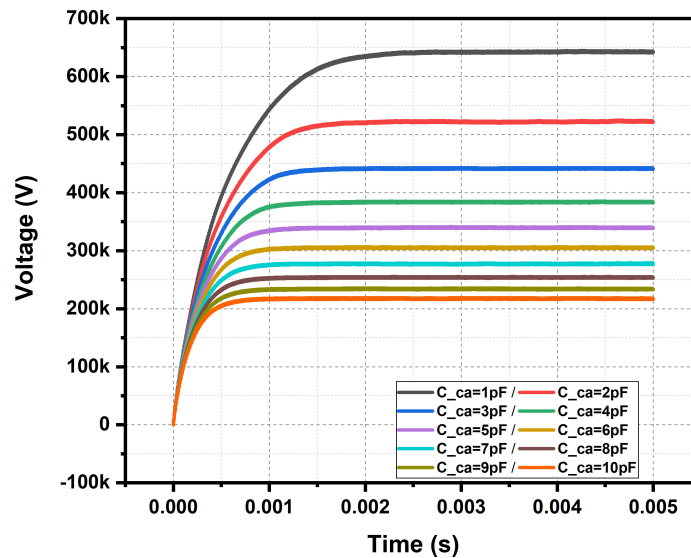

Figure 24. Effect of different amounts of C_{ca} on the amount of the output DC voltage.

The effect of C_f on the output DC voltage is negligible. When C_f increases from 10pf up to 1000pf, the output DC voltage just decreases from 452kV to 439kV. This amount of voltage drop (13kV) is completely negligible against the voltage of the HVT.

We can also see that for values of more than 70pf, the output DC voltage is constant and this situation continues even for the values up to 1000pf. The effect of C_f on the output voltage ripple of HVT has also been shown in figure 26.

According to this simulation, the output voltage ripple has increased from 13kV to 23kV. For values of more than 80pf, the ripple stays constant even for values up to 1000pf.
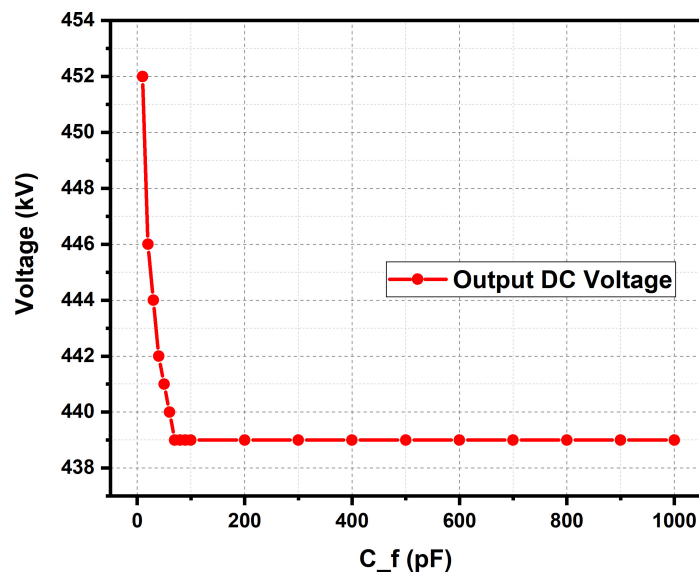
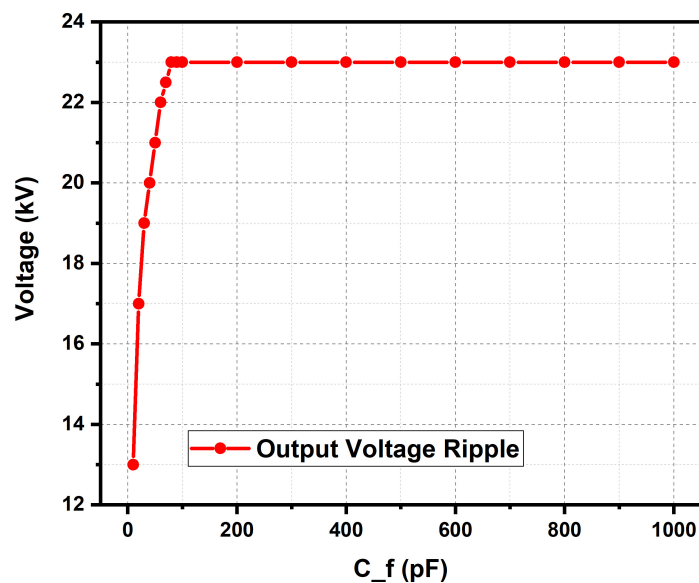**Figure 25**. Effect of the capacitance of C_f on the HVT output DC voltage.

Figure 26. Effect of C_f on the output voltage ripple.

In fact, this parameter is an important factor in the total capacitance of the VMC circuit. It can affect on the resonance frequency of the accelerator. Figure 27 shows the designed circuit to achieve the results and simulations of the figures of 23 to 28.

At the end of the PSpice simulations and with respect to the results of the diagrams, mechanical restrictions and our achievable diode characteristics, the optimum values of the studied parameters were selected. Table 4 shows the optimum values of the different capacitances of the VMC.
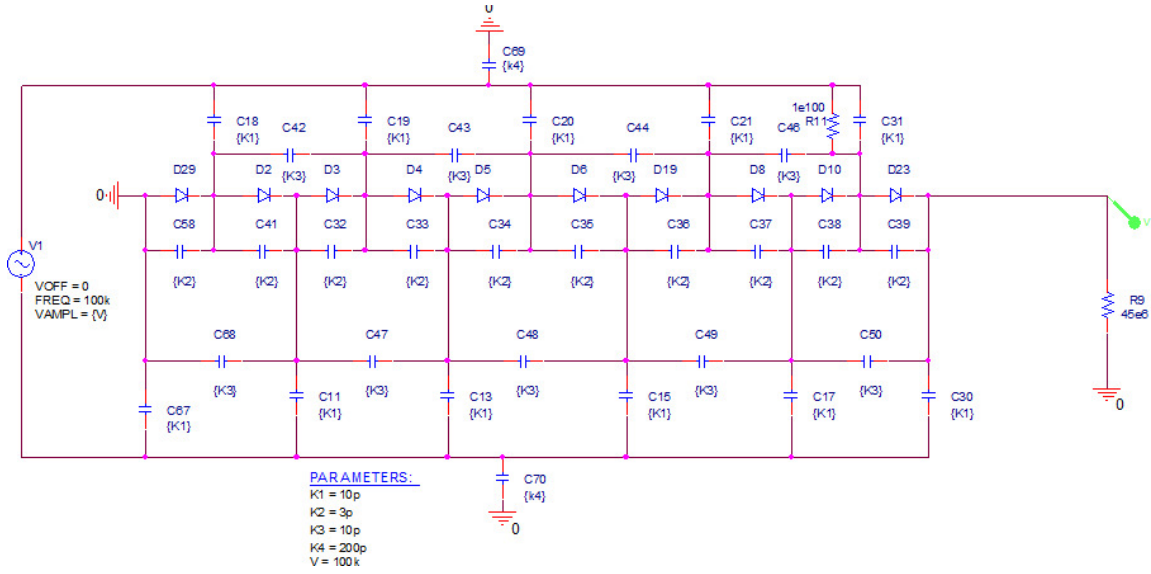
Figure 27. Full view of our designed circuit to achieve the optimum values.

Table 4. Optimum values of the different capacitors.

parameter	value
C_{se}	10
C_{ca}	3
C_{cc}	20
C_f	500–1000

5.2 Calculation of number of the stages of the VMC

For calculating the number of the stages of this circuit, the equations of (4.1), (4.2), (4.3) and (4.4) should be solved for the values of 1MeV and 100mA.

The optimum values achieved by PSpice and CST simulations for C_{ca} (with respect to the diode junction and corona cap capacitances) and C_{se} are respectively 3pf and 10pf. Therefore, the coupling coefficient can be calculated by the equation (4.4):
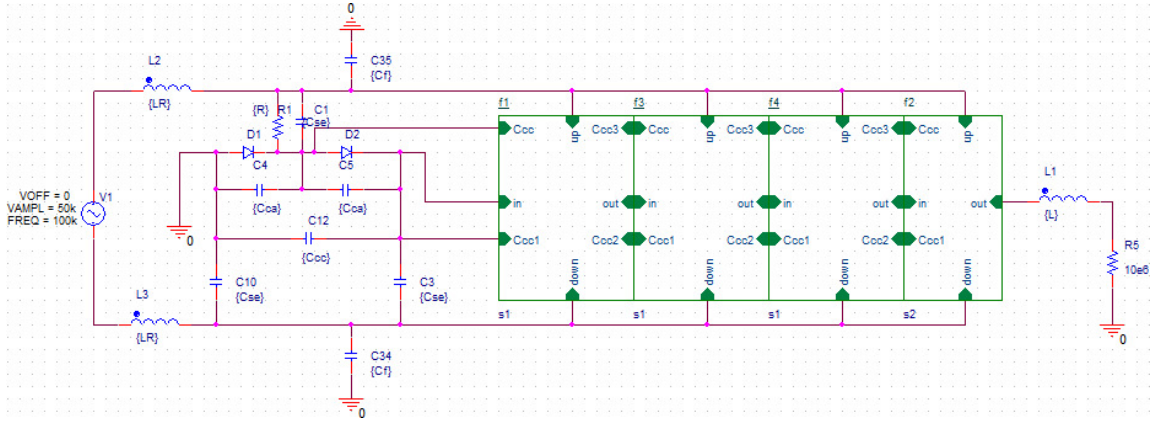
$$k = 1 + 4\frac{C_{Ca}}{C_{Se}} = 2.2$$

Now with respect to different parameters of table 5, we can start to calculate the voltage ripple, droop voltage and number of the stages. The output of these equations for the voltage ripple and number of the stages of VMC is 50kV and 42 stages respectively.

This is a large amount of ripple and in practice, we will reduce it by some technics and filters.

Figure 28 shows the designed circuit of our 1MeV, 100mA multiplier circuit. Every Block contains 10 stages. In practice, the input RF voltage will be 50kV and will increase by the resonance selves up to 150kV in the resonance condition.

Table 5. Parameter values of a 1MeV, 100mA VMC.

parameter	value
f	100kHz
C_{se}	10pf
k	2.2
I	100mA
U_0	150kV
U	1MeV

Figure 28. 42 Stage designed circuit of 1MeV, 100mA multiplier column.

5.3 Final check of VMC outputs

After replacing the values of the table 5 into the simulated circuit of the figure 28, we can drive the output results of current and DC voltage of the VMC. In these simulations, the load current was 10MΩ and the number of stages was 42. Figure 29 shows the output ripple and DC voltage of the 1MV and 100mA designed circuit.

PSpice simulation shows almost the same result (1050kV) as the theoretical calculations (1000kV). The extra amount of 50kV is because of the effect of the capacitances of C_f and C_{cc}. according to the equation (4.3), the voltage ripple is independent of the number of the stages. The result of the output current of this circuit has been shown in figure 30.

These results show a good agreement between the simulations and the theoretical values. Now we can take our optimum parameters of the PSpice simulations into CST Particle Studio for the next step.

5.4 Mechanically designing of the accelerator

The optimum capacitances will be made by metallic (stainless steel or aluminium) electrodes. Diode stacks have also a special structure. For supporting the diodes from the astray electric fields and accelerated charged particles, every diode should be supported by a special supporting case
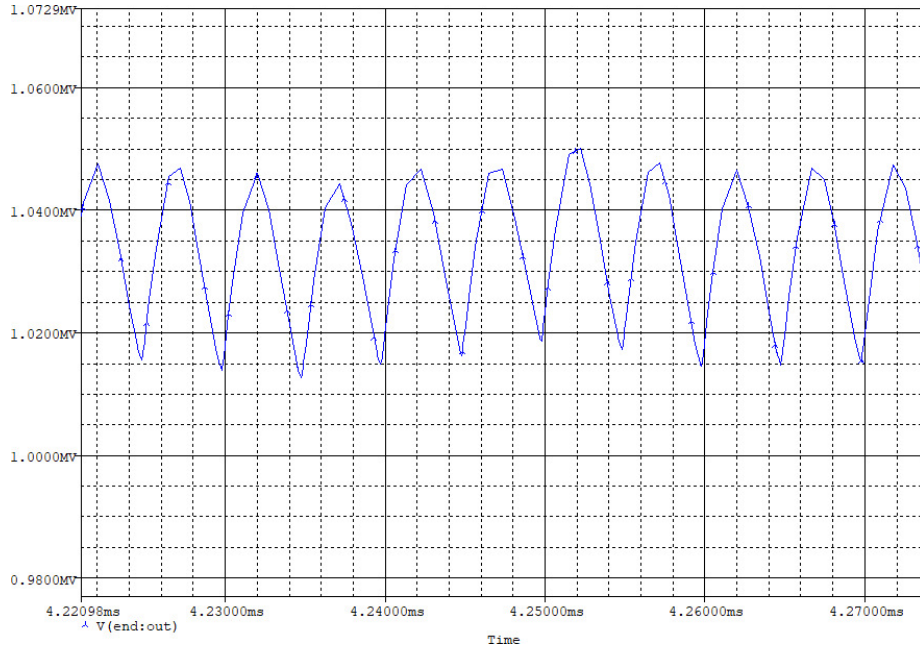
– 23 –

Figure 29. Output ripple and DC voltage of the 42 stage circuit.
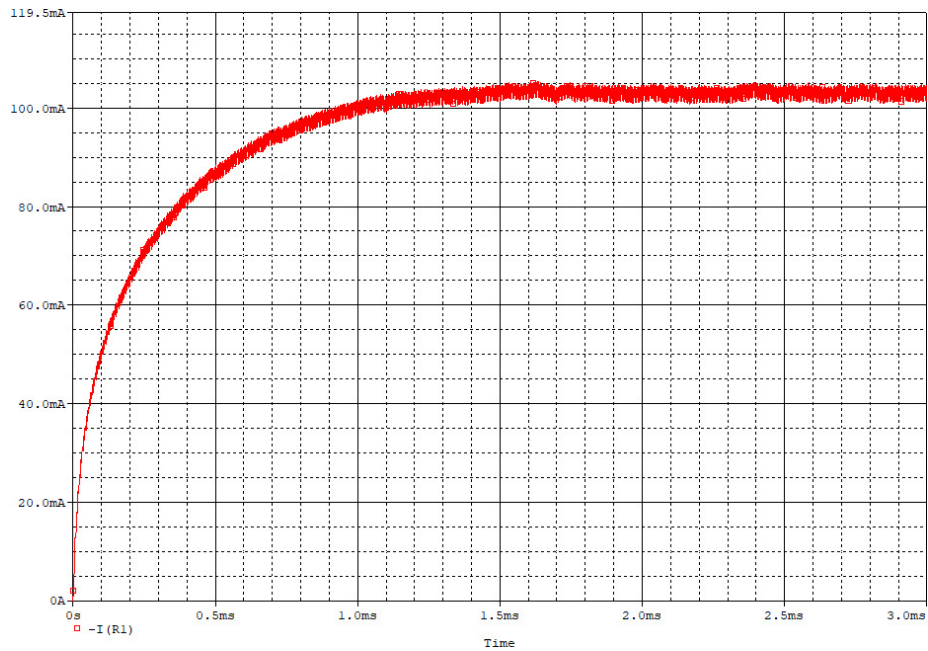

Figure 30. PSpice result for output current of the 42 stage circuit.

(aluminium, stainless steel or brass) [31, 32]. Figure 31 shows our designed stack diode with the supporting aluminium corona caps.

After designing the diode stacks, electron gun and accelerating tube, the characteristics and dimensions of the other electrodes can also be achieved. The length and diameter of the accelerating tube and diode stacks determine the inner diameter of the corona guards. Figure 32 shows the designed corona ring electrode.
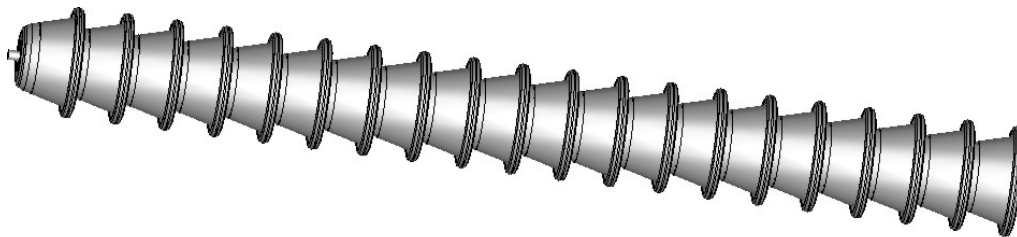
Figure 31. A diode stack with the corona caps for shielding of the diodes.
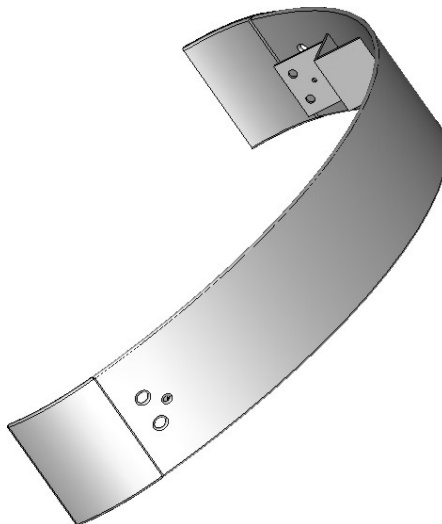

Figure 32. The designed corona guard electrode.

This electrode has been designed in order to create the required capacitances (calculated by PSpice simulations). These electrodes should also be easily mountable on the Plexiglas frame. Figure 33 shows a full view of 43 Nos. of designed corona guards that have been fixed next to each other.
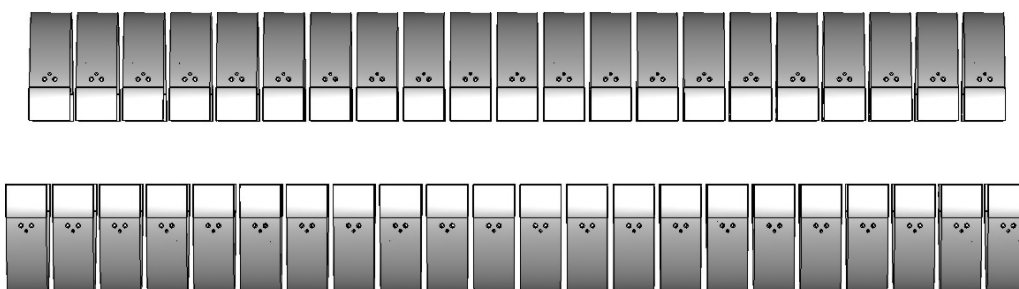

Figure 33. Set of 43 designed corona guard electrodes of 1MeV, 100mA VMC.

The distances between two consecutive electrodes are 13mm (with respect to the voltage breakdown limits and required capacitances). Also these electrodes have the Width of 8cm and the thickness of 3mm. The difference potential between every electrode with a front side electrode is about 50kV. Therefore, the edges of the electrodes should be completely bent and polished not to create the electric discharges [33].
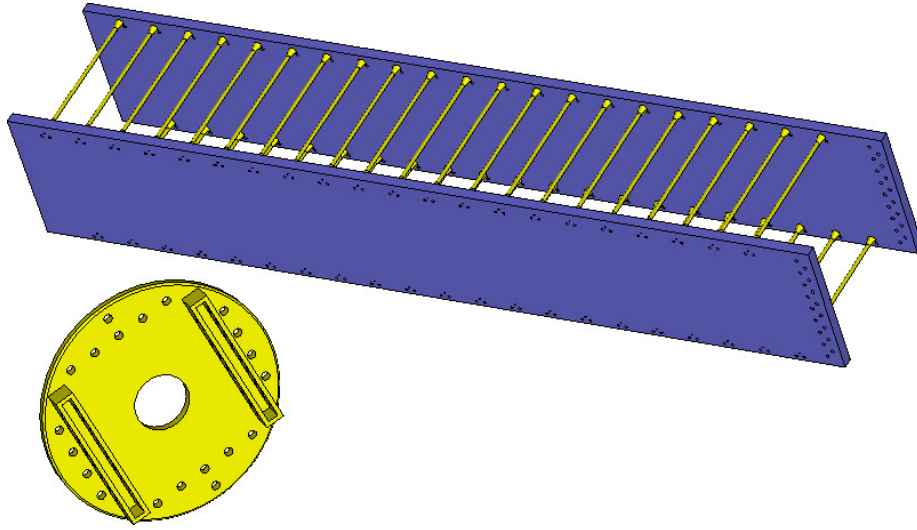
Figure 34. The designed Plexiglas frame and its aluminum holder.

The other important part of the VMC is the holder Plexiglas frame. This part should be designed with enough mechanical strength, life span, dielectric strength and should be lightweight. Figure 34 shows the designed frame.

This frame contains two rectangular sheets of Plexiglas with the thickness of 2.5cm. Yellow aluminum rods have been mounted between two sheets to increase the mechanical strength of the frame. The distance between consecutive rods is 9cm.

The other yellow aluminum circular clamp is a jaw for keeping the frame sheets and mounts those at the bottom of the tank body (by a stainless steel clamp). After installing the frame, we can set the diode stacks on it. The diode stacks have been screwed to the frame and the corona guards. Every diode stack and corona guard has also been electrically connected to the nearest aluminum rod. In fact, all of the diode stacks have been serially connected to each other. Figure 35 shows the array of the diode stacks, mounted on the designed frame. In addition, figure 36 shows the mounted HVT on a stainless steel holder frame at the top of the Plexiglas frame.

These structures will be mounted to the pressure vessel by a stainless steel clamp. This stainless steel clamp has been shown in figure 37.

Central aperture of this clamp is an output for the accelerating tube. After designing and assembling of all parts to each other, a full view of the inner part of the VMC has been shown in figure 38.

The electron gun and the accelerating tube have also been mounted between the Plexiglas sheets. The designed pressure vessel has also three parts; base, middle and the ending section.

For achieving the required capacitances of C_{se} and C_f, DEE electrodes have been designed with the radius of 55cm. Figure 39 shows the designed DEE electrodes.

For placing every electrode at the inside of the pressure vessel, two dielectric rails (PTFE) have been screwed into the pressure vessel. Figure 40 shows the middle part of the pressure vessel, screwed dielectrics and DEE electrodes.

Figure 41 shows a full view of the different parts of our designed industrial parallel-fed Cascade accelerator. This accelerator has the length of 2.9m and the diameter of 1.4m.
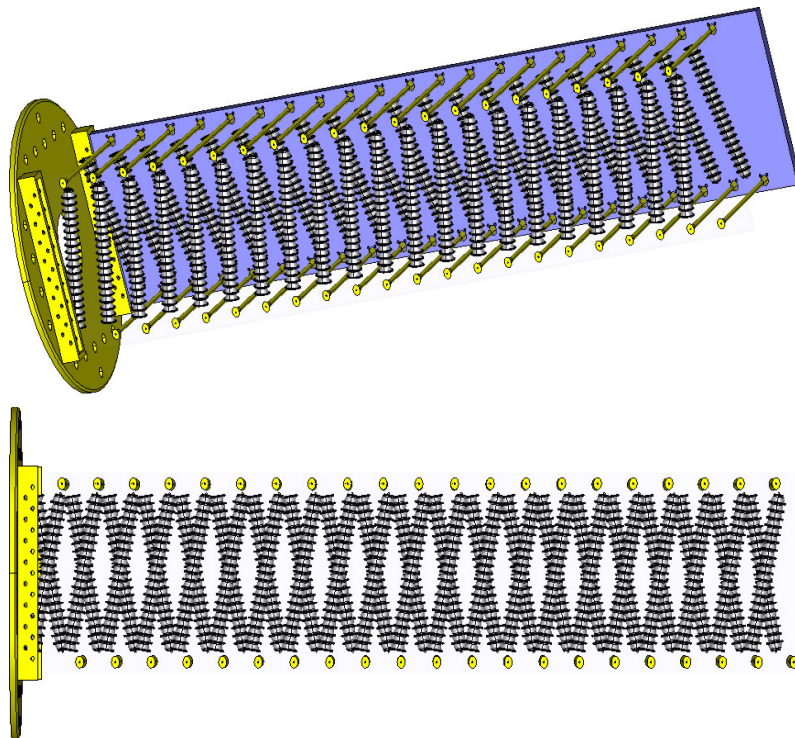
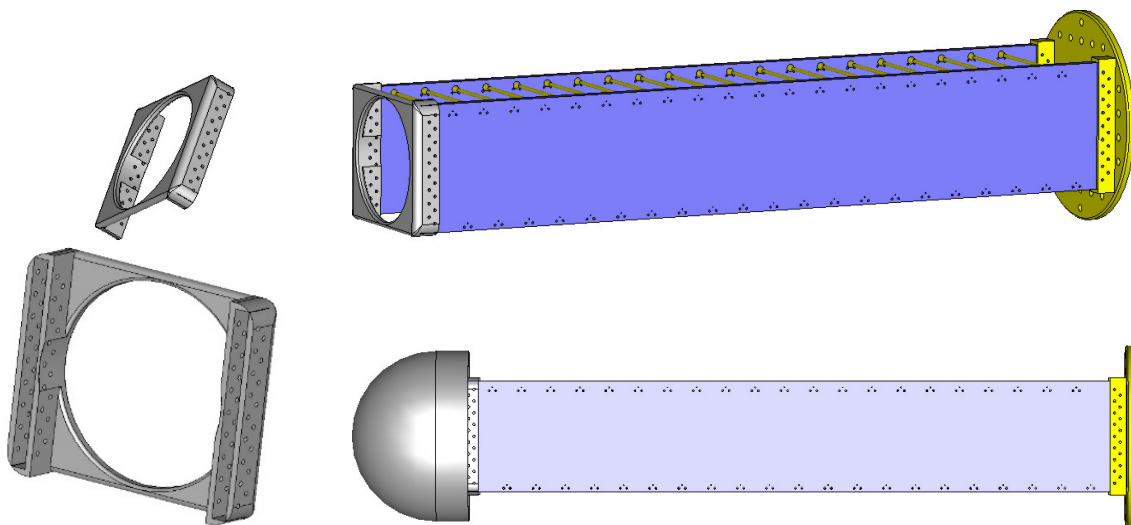**Figure 35**. Mounted diode stacks on the holder frame.

Figure 36. Design of HV terminal and its stainless steel holder frame at the top of the Plexiglas frame.

6   Conclusion

We have made a decision to construct a Parallel-fed capacitive coupled cascade accelerator. We
have selected it because of simplicity, high amount and wide range of beam current, cheapness and
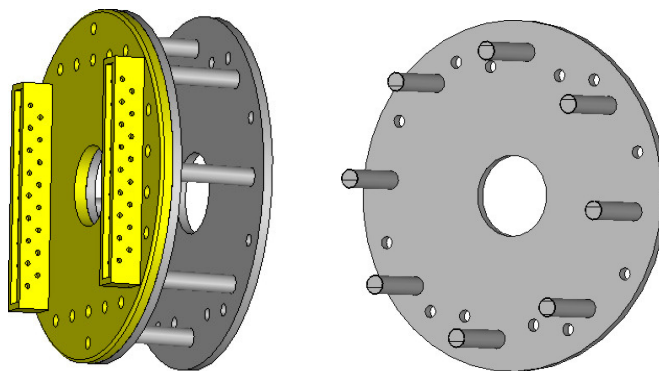
Figure 37. The designed stainless steel clamp for mounting the VMC on the pressure vessel.
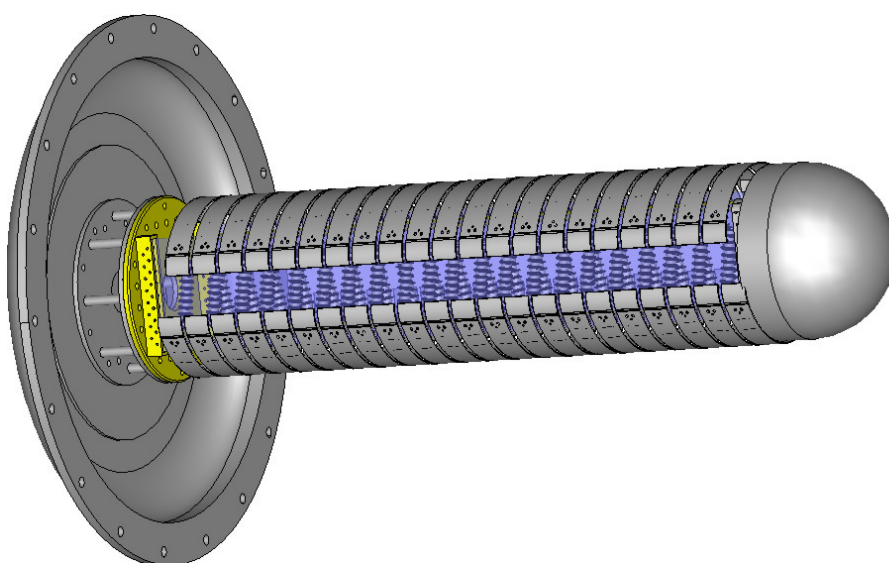

Figure 38. Central part of the 1MeV, 100mA VMC and its different parts.
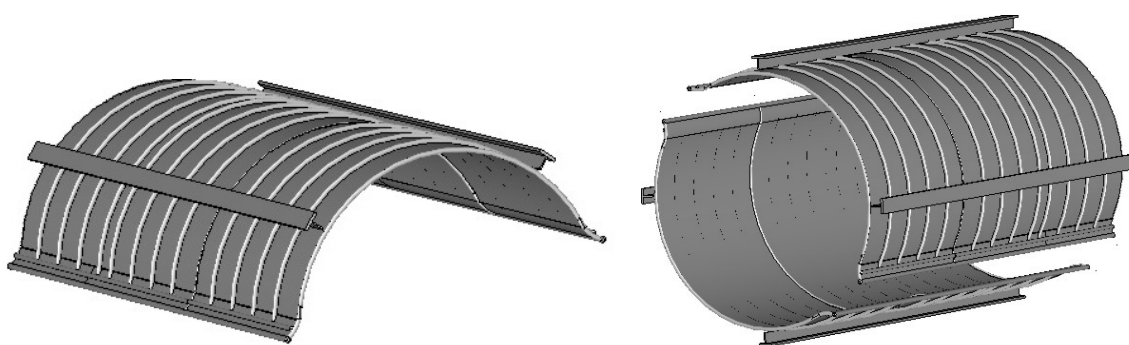

Figure 39. The designed DEE electrodes.

covering many areas of applications. Different components of this machine including two type of electron guns and three type of accelerating tubes were designed and compared. Both of the flat
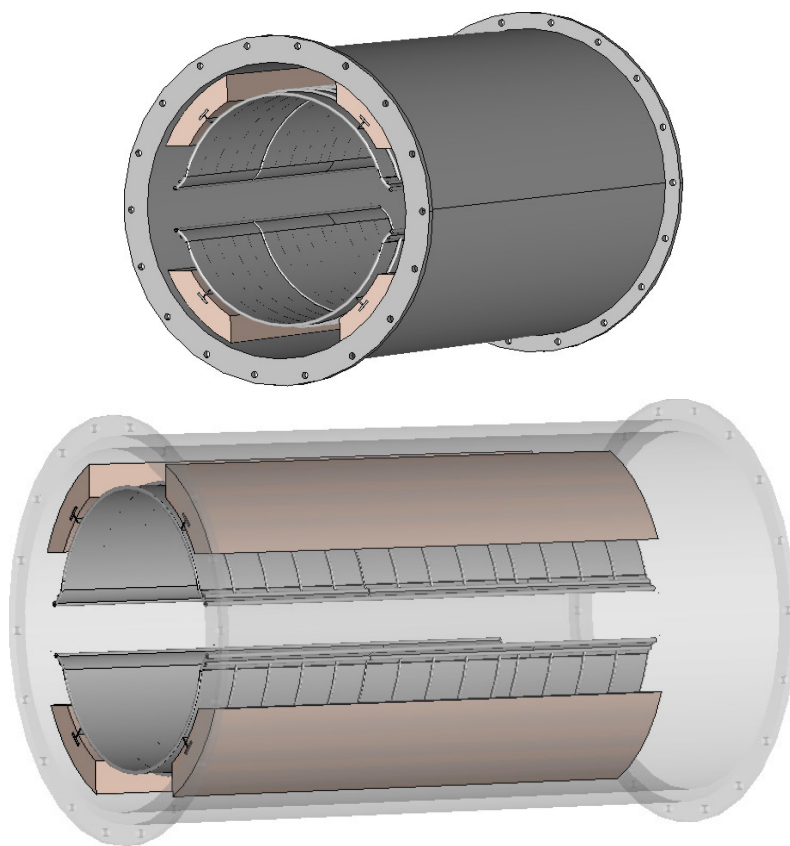
Figure 40. Middle part of the designed pressure vessel, screwed dielectrics and DEE electrodes.

cathode and the spherical cathode guns can be used for industrial DC electron accelerators. We selected the flat cathode due to aforementioned reasons.

Different types of accelerating tubes with different electrode geometries can also be used for an industrial DC accelerator. The best choice is a tube with the most uniform electric field distributions and the most effective coverage of the insulators of the tube. The geometry of the electrodes should be designed with the least sharp points and should cover the insulators against the particle collisions. For optimizing performance of the VMC, different parameters of the VMC should be optimized with PSpice simulations. For these optimizations, many compromises must be considered among different parameters. Some of these parameters are different capacitances, maximum sustainable reverse voltage of every diode stacks, amplitude and frequency of the input RF voltage and the maximum electric field density among the different electrodes. The VMC comprises 42 Nos. of diode stacks and 43 Nos. of corona guards. At the end, all of the designed components were assembled and the whole manner of constructing these kind of accelerators was shown. The designed accelerator can produce a 1MeV, 100mA beam current.
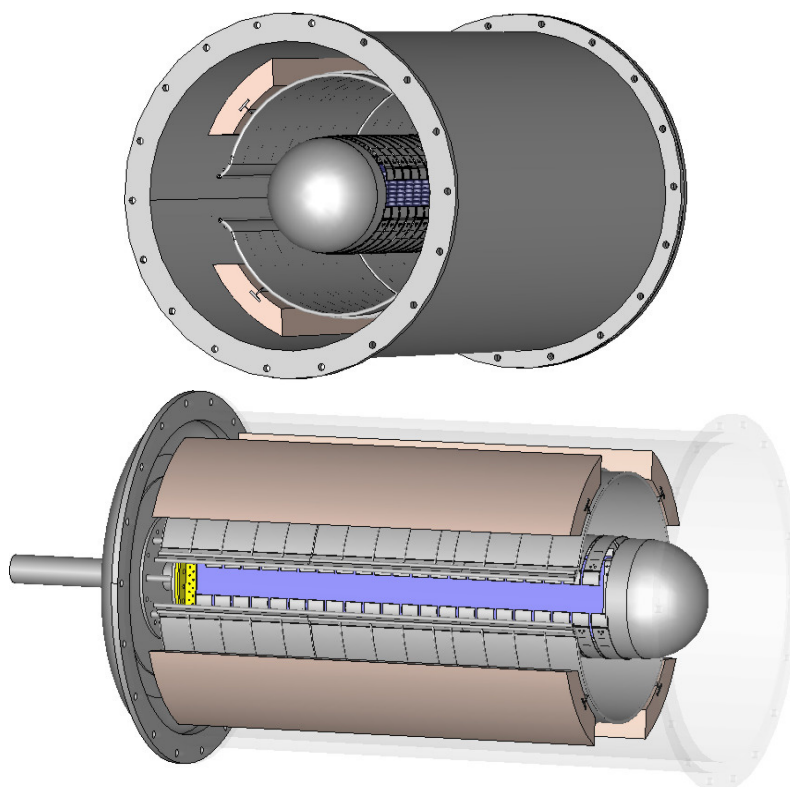
Figure 41. Different views of our designed industrial parallel fed Cascade accelerator.

References

[1] R. Galloway, T. Lisanti and M. Cleland, *A new 5MeV–300 kW dynamitron for radiation processing*, *Radiat. Phys. Chem.* **71** (2004) 551.

[2] M.R. Cleland, *Industrial applications of electron accelerators*, CERN-2006-012, (2006).

[3] R.A. Galloway, S. DeNeuter, T.F. Lisanti and M.R. Cleland, *The new IBA self-shielded dynamitron accelerator for industrial applications*, *AIP Conf. Proc.* **680** (2003) 977.

[4] B. Nayak et al., *1 MeV, 10 kW DC electron accelerator for industrial applications*, 2016 *JINST* **11** P03006.

[5] D. Sharma et al., *Performance of 3 MV voltage multiplier for 3 MeV, 30 kW DC electron beam accelerator at EBC, Kharghar*, *Regulation* **10** (2011) 11.

[6] B.D. Foulis, *A gridless, variable perveance Pierce electron gun*, Ph.D. thesis, Department of Electronic Engineering, University of Natal, South Africa (1994).

[7] A.S. Gilmour Jr., *Principles of traveling wave tubes*, Artech House Radar Library, Artech Print on Demand, 1 December 1994.

[8] C.J. Karzmark, C.S. Nunan and E. Tanabe, *Medical electron accelerators*, McGraw-Hill, U.S.A., 1 September 1992 [ISBN-13:978-0071054102].

[9] S. Humphries Jr., *Charged particle beams*, reprint edition, Dover Books on Physics, Dover Publications, U.S.A., 17 April 2013.

[10] M. Chodorow, E.L. Ginzton, W.W. Hansen, R.L. Kyhl, R.B. Neal and W.K.H. Panofsky, *Stanford high-energy linear electron accelerator (mark-III)*, *Rev. Sci. Instrum.* **26** (1955) 134.

[11] A. Jain, A.R. Chindarkar and K.C. Mittal, *Design and operating experience of triode electron guns*, in *APAC* 2007, Raja Ramanna Centre for Advanced Technology (RRCAT), Indore, India (2007).

[12] C. Tang, H. Chen and Y. Liu, *Electron linacs for cargo inspection and other industrial applications*, *International topical meeting on nuclear research applications and utilization of accelerators*, Vienna, Austria, 4–8 May 2009.

[13] C. Nordling and J. Österman, *Physics handbook: for science and engineering*, eighth edition, Studentlitteratur AB, Lund, Sweden (2006).

[14] M. Nazari et al., *Design and simulation of a thermionic electron gun for a* 1 *MeV parallel feed Cockcroft-Walton industrial accelerator*, in 7th *International Particle Accelerator Conference (IPAC'*16*)*, TUPOY032, Busan, Korea, 8–13 May 2016.

[15] M. Nazari et al., *Design, simulation and compare of flat cathode electron guns with spherical cathode electron guns for industrial accelerators*, in *Proceedings of the* 8th *Int. Particle Accelerator Conf. (IPAC'*17*)*, MOPIK075, Copenhagen, Denmark, 14–19 May 2017.

[16] D. Bhattacharjee et al., *Development of electron guns for linacs and DC accelerator*, *J. Phys. Conf. Ser.* **390** (2012) 012071.

[17] T.W. Aitken, *The high voltage test programme at Daresbury for the NSF accelerator*, in *Proc. First Int. Conf. Tech. Electrostatic Accelerators*, DNPL/NSF/R5, Daresbury Laboratory, Daresbury, U.K. (1973), pg. 147.

[18] H.R. Hyder and G. Doucas, *Experiences with suppressed accelerator tubes*, in *Proc. First Int. Conf. Tech. Electrostatic Accelerators*, DNPL/NSF/R5, Daresbury Laboratory, Daresbury, U.K. (1973), pg. 352.

[19] A. Galejs and P.H. Rose, *Optics of electrostatic accelerator tubes*, in *Focusing of charged particles*, volume 2, A. Septier ed., Academic Press, New York, NY, U.S.A. and London, U.K. (1967), pg. 297.

[20] P.T. Brady, *The construction of a* 200 *keV electrostatic accelerator*, B.Sc. thesis, Department of Physics, Houghton College, New York State, U.S.A. (2004).

[21] R. Anderson, *Report on pulsed vacuum breakdown of plexiglass insulators*, Sandia National Laboratory report SAND-75, U.S.A. (1976), pg. 0667.

[22] M. Nazari et al., *Design, simulation and comparison of electrostatic accelerating tubes for a* 1 *MeV parallel feed Cockcroft-Walton industrial accelerator*, in 7th *International Particle Accelerator Conference (IPAC'*16*)*, TUPOY033, Busan, Korea, 8–13 May 2016.

[23] U. Giesen, *The Notre Dame KN accelerator laboratory*, in *Symposium of north eastern accelerator personnel — SNEAP* 32, D.K. Hensley et al., World Scientific, Singapore (2001), pg. 326 [ISBN:9789812811721].

[24] M.A. Plum, *Beam loss and accelerator protection*, in *Proceedings of the* 2014 *joint international accelerator school: beam loss and accelerator protection*, CERN-2016-002, Newport Beach, CA, U.S.A., 5–14 November 2014.

[25] F. Hinterberger, *Electrostatic accelerators*, CERN-2006-012, (2006).

[26] C. Dwivedi and M. Daigvane, *Multi-purpose low cost DC high voltage generator (*60 *kV output), using Cockcroft-Walton voltage multiplier circuit*, in 2010 3rd *International Conference on Emerging Trends in Engineering and Technology*, IEEE, (2010).

[27] M.R. Cleland and P. Farrell, *Dynamitrons of the future*, *IEEE Trans. Nucl. Sci.* **12** (1965) 227.

[28] M. Nazari et al., *Design and simulation of voltage multiplier column of a* 300 *keV,* 10 *mA parallel fed Cockcroft Walton electron accelerator for industrial applications*, in 8th *International Particle Accelerator Conference (IPAC'*17*)*, Copenhagen, Denmark, 14–19 May 2017.

[29] C. Thompson and M. Cleland, *High-power dynamitron accelerators for X-ray processing*, *Nucl. Instrum. Meth.* **B 40-41** (1989) 1137.

[30] W. Shen, *Design of high-density transformers for high-frequency high-power converters*, Ph.D. thesis, Virginia Tech, Blacksburg, VA, U.S.A. (2006).

[31] D. Sharma et al., *Design of rectifier stacks and its protection scheme for* 3 *MV voltage multiplier*, in *Proceedings of the Indian particle accelerator conference*, (2013).

[32] S. Dewangan, D. Sharma and R. Bakhtsingh, *Development of high voltage surge limiting resistor for protection of HV multiplier of* 3 *MeV DC accelerator*, in *Proceedings of the Indian particle accelerator conference*, (2013).

[33] D. Sharma et al., *HV support structure of* 3 *MVDC generator and its protection from HV discharges in vacuum and SF*6 *gas for DC electron accelerator*, in 2014 *International Symposium on Discharges and Electrical Insulation in Vacuum (ISDEIV)*, IEEE, (2014).